Electronic Supplementary Material (ESI) for Polymer Chemistry.

Electronic Supplementary Information (ESI):

Discotic columnar liquid crystalline polymer semiconducting materials with high charge-carrier mobility via rational macromolecular engineering

Bin Mu,[a] Xingtian Hao,[b] Jian Chen,[a] Qian Li,[a] Chunxiu Zhang,[b] and Dongzhong Chen*[a]

[a] *Key Laboratory of High Performance Polymer Materials and Technology of Ministry of Education, Collaborative Innovation Center of Chemistry for Life Sciences, Department of Polymer Science and Engineering, School of Chemistry and Chemical Engineering, Nanjing University, Nanjing 210023, China*

**E-mail: cdz@nju.edu.cn*

[b] *Information Recording Materials Lab, Lab of Printing & Packaging Materials and Technology, Beijing Institute of Graphic Communication, Beijing102600, China*

Table of contents

1. Molecular characterization of the series DLC polymers ^4P_m-*n* with GPC and NMR

Gel-permeation chromatography (GPC) measurements were performed at 25 ℃ on a Waters 515 equipped with Wyatt Technology Optilab rEX differential refractive index detector. THF was used as the eluent at a flow rate of 1.0 mL min^{-1}, the solvent THF and sample solutions were filtered over filters with pore size of 0.45 μm (Nylon, Millex-HN 13 mm Syringes Filters, Millipore, US). Relative weight average (M_w) and number average (M_n) molecular weights were calculated based on a group of polystyrene standard samples. It is noteworthy that though the molecular weights (MWs) of oligomeric ^4P_m-10 determined by GPC showed small deviation from the theoretical molecular weight, while the MWs of high-DP polymers ^4P_m-50 were significantly underestimated by GPC (Table S1), which was ascribed to the strong contraction behaviour of high-DP DLC polymers in solution correlated closely with their various self-organized structures in bulk as revealed for the ^6P_m-n series in our previous reports.[1,2]

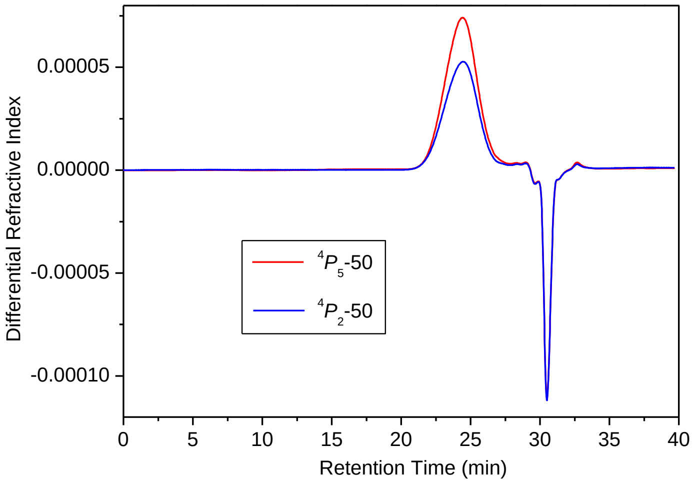

Figure S1. Representative monomodal GPC curves of $^4P_2$-50 and $^4P_5$-50 revealing highly pure high-molecular-weight DLC polymers after purifying the products of RAFT polymerization through column chromatography to preclude any possible contamination from unreacted residual monomers and other low molar mass discotic compounds.

The MWs of DLC polymers with relatively longer spacers and low-DP can be well estimated through integral ratio of characteristic ^{1}H NMR peaks (Table S1, Fig.S2a), while the MWs of those with shorter spacers, even for low-DP samples, can not be obtained via NMR spectra because the end-group peaks for calculation reference is overlapped by the broadened and partially branched alkoxy peaks resulting from discotic mesogen-jacketed effect (Fig.S2b, Table S1). The MW of one of the high-DP DLC polymers with a longer six-methylene spacer $^4P_6$-50 is estimated to be 34000, in good agreement with the designed value. Although the MWs of other polymer samples with shorter spacers and/or high-DP can not be estimated from NMR spectra, their generally in agreement with the designed value should be reliable based on the previously demonstrated well-controlled RAFT polymerization method[1,2] and the high monomer conversion for all polymerization reactions.

Table S1. Molecular characterization results of ^4P_m-n series via GPC and NMR.

^4P_m-10	$^4P_1$-10	$^4P_2$-10	$^4P_3$-10	$^4P_4$-10	$^4P_5$-10	$^4P_6$-10
$M_{w,GPC}$ [g mol^{-1}]	6,100	6,300	6,600	7,400	6,700	8,400
PDI	1.28	1.22	1.24	1.23	1.17	1.29
$M_{n,NMR}$ [g mol^{-1}]	/ [a]	/ [a]	/ [a]	7,000	7,200	7,500
^4P_m-50	$^4P_1$-50	$^4P_2$-50	$^4P_3$-50	$^4P_4$-50	$^4P_5$-50	$^4P_6$-50
$M_{w,GPC}$ [g mol^{-1}]	11,600	10,800	12,400	10,900	10,800	14,800
PDI	1.46	1.41	1.42	1.31	1.32	1.40
$M_{n,NMR}$ [g mol^{-1}]	/ [a]	/ [a]	/ [a]	/ [a]	/ [a]	34,000

[a] Not available by integral ratio of characteristic ^{1}H NMR peaks due to overlapped peaks resulting from too high molecular weight or discotic mesogen-jacketed effect in those DLC polymers with short spacers as shown in Figure S2b.

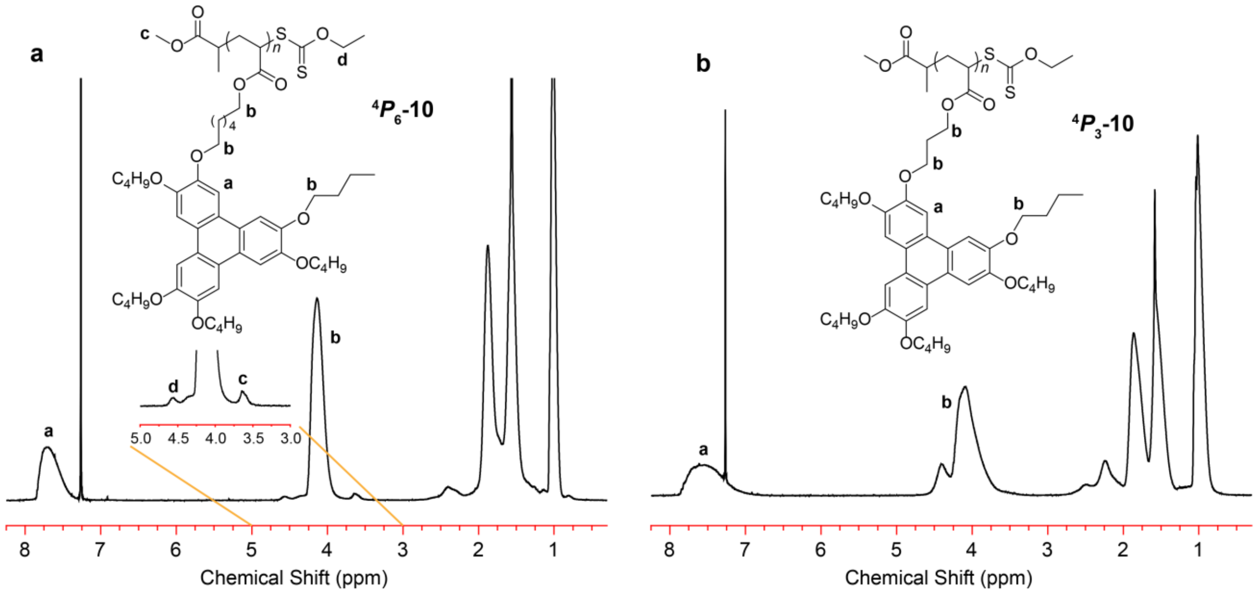

Figure S2. Representative ^{1}H NMR spectra of DLC polymers: (**a**) with relatively longer spacers and low-DP such as $^4P_6$-10, the molecular weights can be well estimated through integral ratio of characteristic peaks, while (**b**) with shorter spacers such as $^4P_3$-10, even for low-DP samples, molecular weights can not be obtained via NMR estimation due to overlapped peaks resulting from discotic mesogen-jacketed effect.

2. Thermal analysis of the series DLC polymers $^{4}P_{m}$-n with DSC

Differential scanning calorimetry (DSC) thermograms were recorded on a Perkin-Elmer Pyris I calorimeter equipped with a cooling accessory and under an argon atmosphere. Transition temperatures were taken as median values for step-shaped glass transitions and peak values for all other transitions from DSC heating or cooling runs at a rate of 10 ℃ min^{-1}.

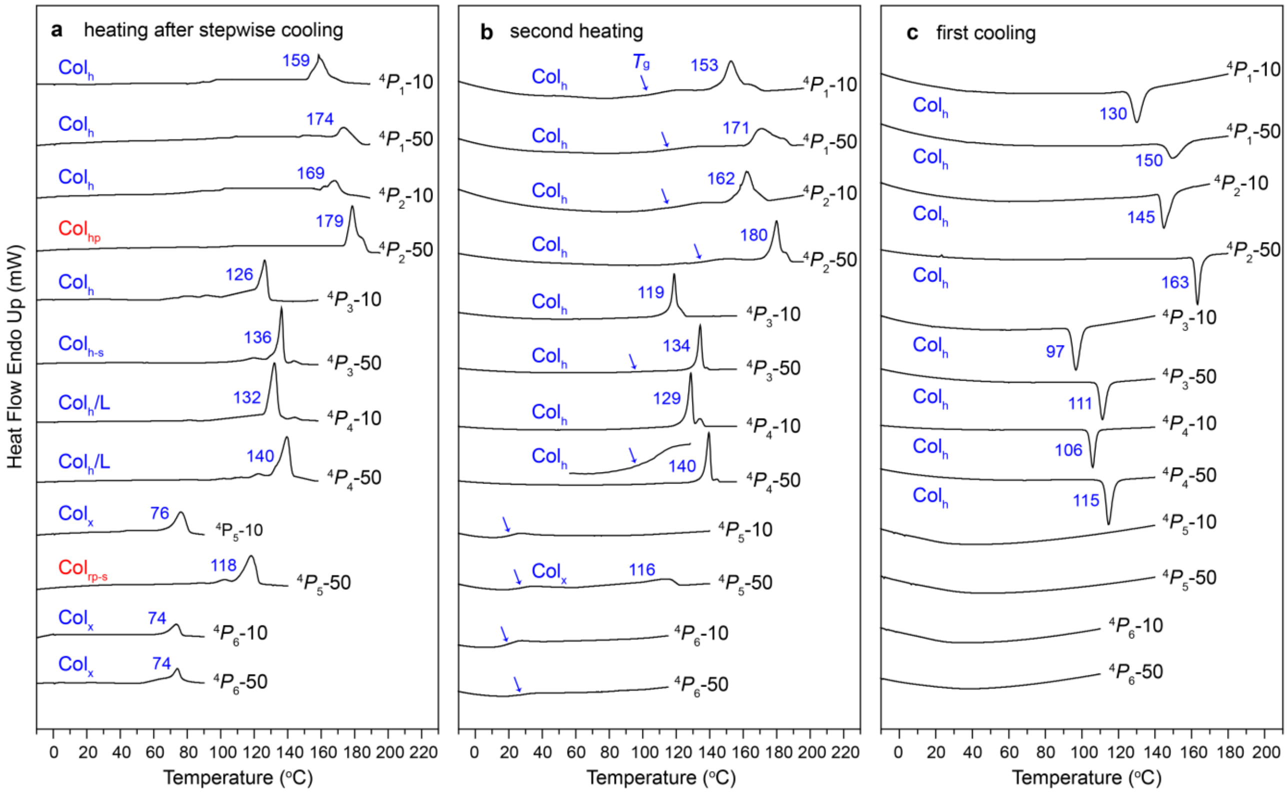

Figure S3. DSC traces of the series side-chain DLC polymers $^{4}P_{m}$-n with variant length spacers m = 1-6, upon first cooling, second heating runs, or heating after a stepwise cooling process,[‡] with a heating or cooling rate of 10 ℃ min^{-1}. Col$_{\mathrm{h}}$ = hexagonal columnar lattice; Col$_{\mathrm{hp}}$ = hexagonal columnar plastic phase; Col$_{\mathrm{h\text{-}s}}$ = hexagonal columnar superlattice; Col$_{\mathrm{h}}$/L = hexagonal columnar lattice with some lamellar correlation; Col$_{\mathrm{rp\text{-}s}}$ = rectangular columnar plastic superlattice; Col$_{\mathrm{x}}$ = unidentified columnar phase. The arrows indicate the glass transition temperature (T_{g}) extracted from the second heating DSC runs or their enlarged curves.

[‡] The *stepwise cooling* process was performed through isothermal annealing for 2~5 hours at each selected temperature about 10 ℃ interval step-down from isotropic melts to room temperature, essentially equivalent to a very slowly cooling process.

Table S2. Thermal data of $^{4}P_{m}$-n extracted from second heating and first cooling runs.

polymer code	thermal transitions/ ℃ (enthalpy changes/J g^{-1})^{a}	
	second heating^{b}	first cooling^{b}
$^{4}P_{1}$-10	G 103 Col$_h$ 153(5.4) I	I 130(-5.9) Col$_h$
$^{4}P_{1}$-50	G 114 Col$_h$ 171(6.5) I	I 150(-6.5) Col$_h$
$^{4}P_{2}$-10	G 115 Col$_h$ 162(7.0) I	I 145(-7.6) Col$_h$
$^{4}P_{2}$-50	G 135 Col$_h$ 180(8.4) I	I 163(-8.9) Col$_h$
$^{4}P_{3}$-10	Col$_h$ 119(6.9) I	I 97(-6.4) Col$_h$
$^{4}P_{3}$-50	G 94 Col$_h$ 134(8.2) I	I 111(-7.6) Col$_h$
$^{4}P_{4}$-10	Col$_h$ 129(9.1) I	I 106(-10.4) Col$_h$
$^{4}P_{4}$-50	G 95 Col$_h$ 140(12.6) I	I 115(-11.5) Col$_h$
$^{4}P_{5}$-10	G 21 I	
$^{4}P_{5}$-50	G 28 Col$_x$ 116(1.6) I	
$^{4}P_{6}$-10	G 19 I	
$^{4}P_{6}$-50	G 27 I	

^{a}Abbreviations: G = glassy state; Col$_h$ = hexagonal columnar lattice; Col$_x$ = unidentified columnar phase; I = isotropic phase. ^{b}The median values for step-shaped glass transitions and peak values for all other transitions obtained from DSC heating or cooling runs at a rate of 10 ℃ min^{-1}, with positive enthalpy changes standing for endothermic while negative values for exothermic transitions.

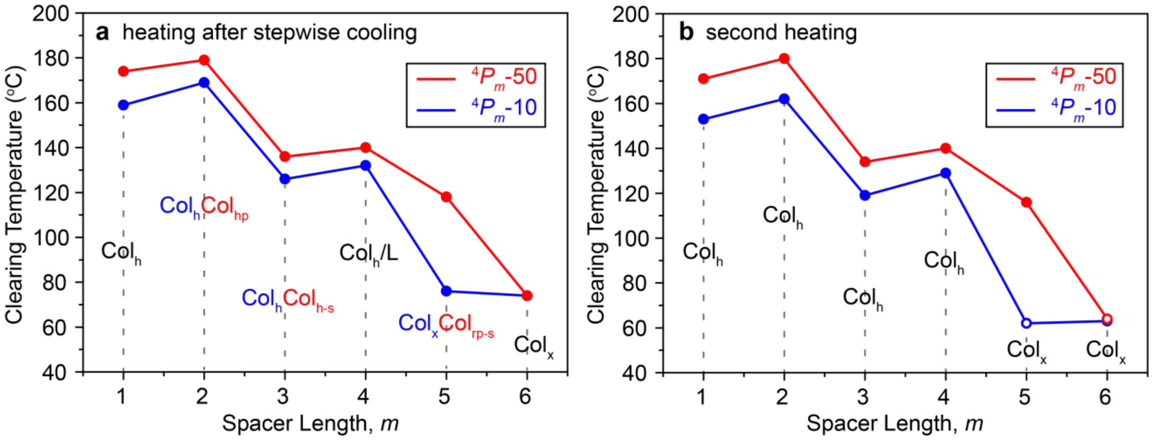

Figure S4. The clearing temperatures versus the spacer length m of $^{4}P_{m}$-n with DP n = 10 or 50 determined from DSC at a heating rate of 10 ℃ min^{-1} during (a) heating after a stepwise cooling process and (b) second heating after a normal cooling at a rate of 10 ℃ min^{-1}, where the empty symbols in (b) indicated transition temperatures from first heating runs instead due to absence of thermal transition signals in the second heating process.

3. Structure characterization and phase assignments of the series $^4\boldsymbol{P_m}$-***n*** with X-ray scattering analysis

X-ray scattering experiments were performed with a high-flux small-angle X-ray scattering instrument (SAXSess mc^2, Anton Paar) equipped with Kratky block-collimation system and a temperature control unit (Anton Paar TCS 120 or TCS 300). Both small- and wide-angle X-ray scattering (SAXS/WAXS) were simultaneously recorded on an imaging-plate (IP) at 40 kV and 50 mA, extending to high-angle range with the scattering vector q range covered by the IP was from 0.06 to 29 nm^{-1}, $q = 4\pi\sin\theta/\lambda$, where 2θ is the scattering angle and the wavelength $\lambda = 0.1542$ nm is of Cu-Kα radiation. The DLC polymer powder samples encapsulated with aluminum foil were used for X-ray scattering analyses, except for the pattern as shown in Figure 2e of main text was collected from the aligned film of sandwiched preparation. The obtained X-ray scattering data were processed with the associated SAXSquant software 3.80 and the aluminum foil background signal was subtracted.

All the small- and wide-angle X-ray scattering (SAXS/WAXS) profiles provided in the following were collected from polymer samples at the same temperature of 50 ℃ during heating process after a cooling process at 10 ℃ min^{-1} or experiencing a stepwise cooling process from their isotropic melts, in agreement with the thermal analysis conditions employed in DSC heating cycles.

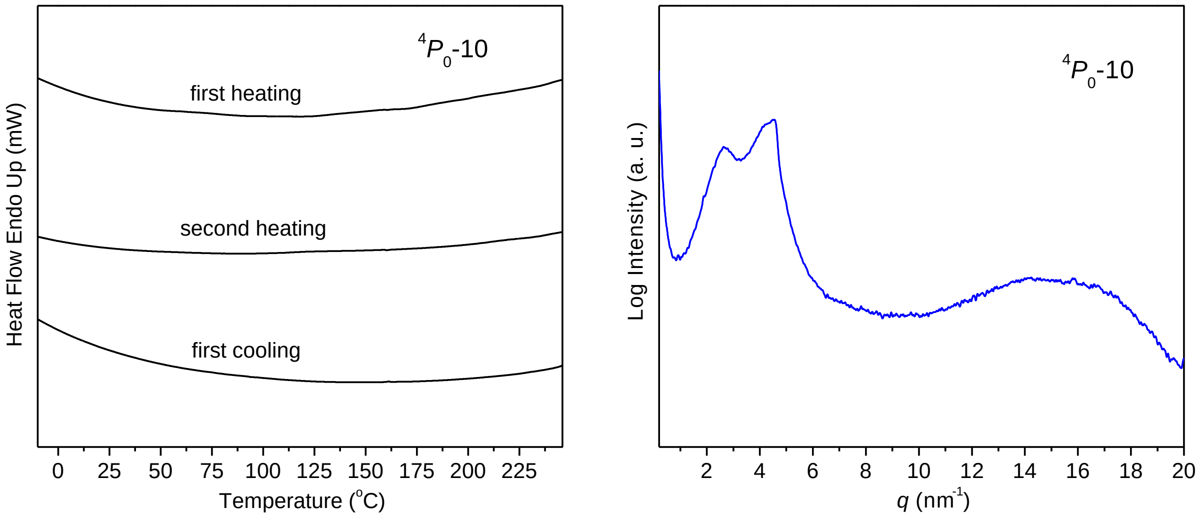

Figure S5. DSC traces at a scanning rate of 10 ℃ min^{-1} and SAXS/WAXS pattern at 50 ℃ obtained from representative $^{4}P_{0}$-10 with the TP discotic side-groups linked to polymer backbone only through an ester group without any methylene spacer.

With the TP discotic side-groups linked to polymer backbone only through an ester group without any methylene spacer, $^{4}P_{0}$-n behaved as discotic mesogen-jacketed LC polymers, which did not exhibit any detectable thermal transitions on either heating or cooling DSC scans, and also no π-π stacking signals were observed in the wide angle region of WAXS patterns (Figure S5).[1,2] All other $^{4}P_{m}$-n DLC polymer samples studied with spacer methylene number m = 1-6 presented obvious diffraction peak around 3.5 Å typical for π-π stacking distance within the columns, and their 2D columnar organization structures are investigated and presented as follows with proposed assignments.

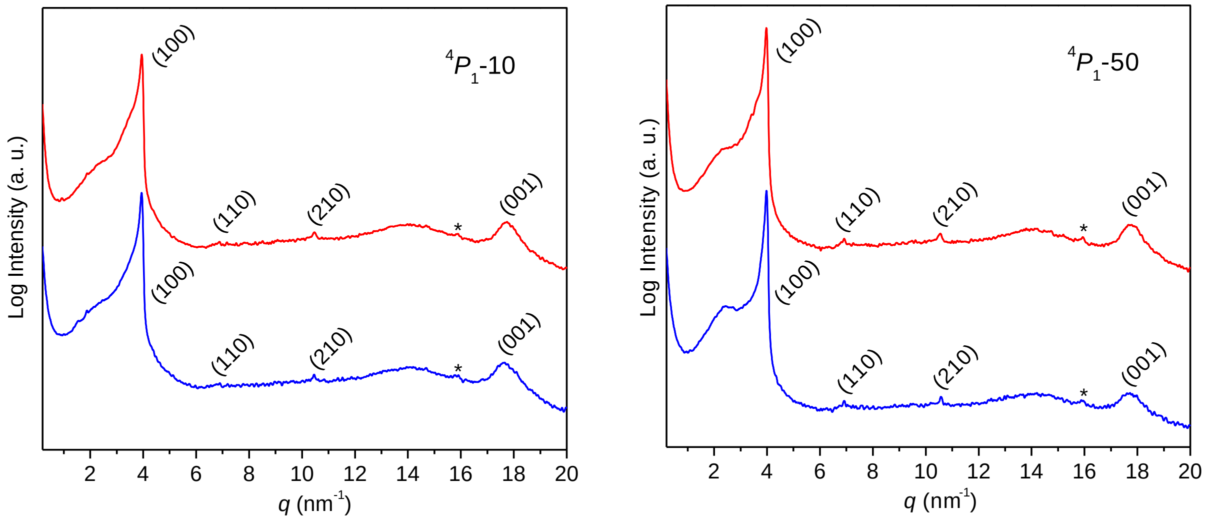

Figure S6. SAXS/WAXS patterns of $^4P_1$-10 and $^4P_1$-50 with proposed indexing at 50 ℃ on cooling from isotropic melts at a rate of 10 ℃ min^{-1} (blue lines) or after a stepwise cooling process (red lines). The shoulder at around 2 nm^{-1} is associated with the degree of compaction and regular arrangement of polymer backbones within the intercolumnar channels, which cannot be clearly ascribed into some superstructures due to lack of higher order scattering signals.

*The background peaks from the packing aluminum foil locating in the wide-angle region are labeled by asterisks, which have a negligible disturbance to the interested sample peaks thus without complete subtraction so as to avoid distortion of the peak shape and smoothing over some significant weak signals, hereinafter the same.

Table S3. Representative SAXS/WAXS data for $^4P_1$-50 at 50 ℃ after a stepwise cooling process.

Meso-phase	*hkl*	d_{obs} [Å]	d_{calc} [Å]	Lattice parameter [Å]	$\rho_{\mathrm{calc}}{}^{a}$ [g cm^{-3}]
Col$_\mathrm{h}$	100	15.9	15.9		
(50 °C)	110	9.17	9.18	a = 18.4	1.10
*p*6*mm*	210	6.00	6.01		
		4.4 (diffuse halo)			
	001	3.53			

^{a}Density, ρ, calculated as $\rho = M \cdot Z/(N_A \cdot V_{\mathrm{unit\ cell}})$, $V_{\mathrm{unit\ cell}} = a^2 \cdot c \cdot \sqrt{3}/2$, where c is experimentally measured d value of (001) scattering peak, M is the molecular weight of the repeat unit of 689 g mol^{-1}, and Z = 1.

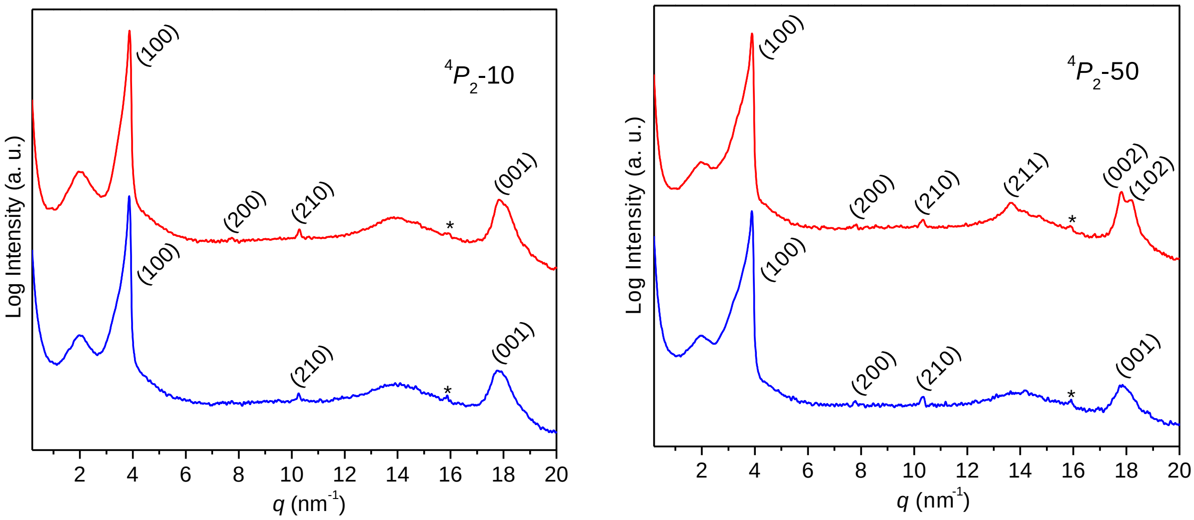

Figure S7. SAXS/WAXS patterns of $^4P_2$-10 and $^4P_2$-50 with proposed indexing at 50 ℃ oncooling from isotropic melts at a rate of 10 ℃ min^{-1} (blue lines) or after a stepwise cooling process (red lines). The broad peak at around 2 nm^{-1} is associated with the degree of compaction and regular arrangement of polymer backbones within the intercolumnar channels, which cannot be clearly ascribed into some superstructures due to lack of higher order scattering signals, hereinafter the same.

Table S4. Representative SAXS/WAXS data for $^4P_2$-50 at 50 ℃ on cooling from isotropic melt at a rate of 10 ℃ min^{-1} (Col$_h$) or after a stepwise cooling process (Col$_{hp}$).

Meso-phase	*hkl*	d_{obs} [Å]	d_{calc} [Å]	Lattice parameter [Å]	$\rho_{calc}{}^a$ [g cm^{-3}]
Col$_{hp}$	100	16.1	16.1		
(50 °C)	200	8.03	8.05	a = 18.6	1.10
*p*6*mm*	210	6.08	6.09		
	211	4.60	4.61		
		4.4 (diffuse halo)			
	002	3.53	3.53		
	102	3.45	3.45		
Col$_h$	100	16.1	16.1		
(50 °C)	200	8.04	8.05	a = 18.6	1.11
*p*6*mm*	210	6.08	6.09		
		4.5 (diffuse halo)			
	001		3.51		

[a] Density, ρ, calculated as $\rho = M \cdot Z/(N_A \cdot V_{unit\ cell})$, $V_{unit\ cell} = a^2\ c \cdot \sqrt{3}/2$, where c is experimentally measured d value of (001) scattering peak (but here (002) peak in Col$_{hp}$ phase), M is the molecular weight of the repeat unit of 703 g mol^{-1}, and $Z = 1$.

With only one methylene spacer, $^4P_1$-n exhibit ordered 2D hexagonal columnar lattice Col$_h$ with lattice parameter a = 18.4 Å both on cooling at 10 ℃ min^{-1} and after a stepwise cooling process from isotropic melts (Figure S6, Table S3). Upon one more methylene elongation, the $^4P_2$-n series, similar to $^4P_1$-n, show ordered 2D Col$_h$ mesophase with lattice parameter a = 18.6 Å on cooling from isotropic melts at 10 ℃ min^{-1} (Figure S6, Table S4). However, after undergoing a stepwise cooling process, $^4P_2$-50 presents a 3D-positionally ordered hexagonal columnar plastic phase Col$_{hp}$ (Figure S7, Table S4). Taking geometric dimension into consideration as shown in Figure S8a,b, for $^4P_2$-n, the extended contour length from the center of TP discogens to polymer backbone is estimated to be 10.95 Å, slightly larger than the X-ray experimentally measured value of 9.3 Å, thus the side-chain TP discotic units stacking alternately in two-column bundles as illustrated in Figure S8b is the most probable and solely permitted way. The $^4P_1$-n series with a shorter spacer but a very similar column diameter to $^4P_2$-n may also take the two-column bundles stacking mode.

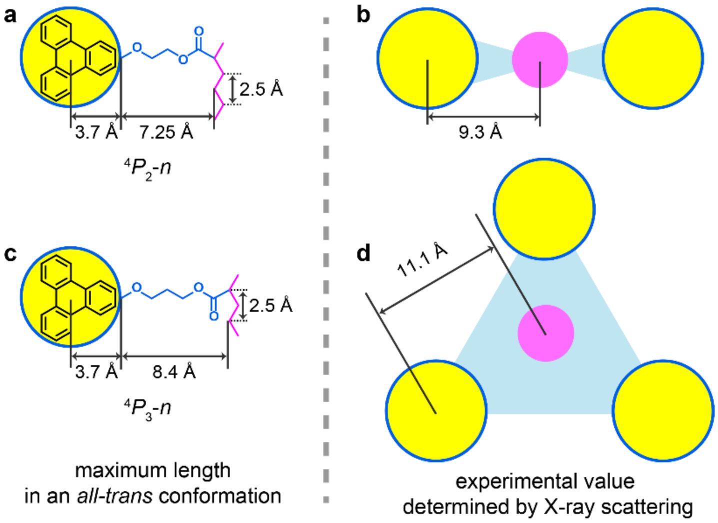

Figure S8. Schematic illustration the geometric dimensions and location of the polymer main chain and pendant TP discogens in the columnar mesophases for $^4P_2$-n and $^4P_3$-n. The dimensions shown on the left side are measured from ChemBio3D Ultra 11.0 with the spacer linkage in an *all-trans* conformation, on the right side is the proposed location of polymer backbone and side-chain TP stacking columns with distances experimentally determined from X-ray scattering analysis.

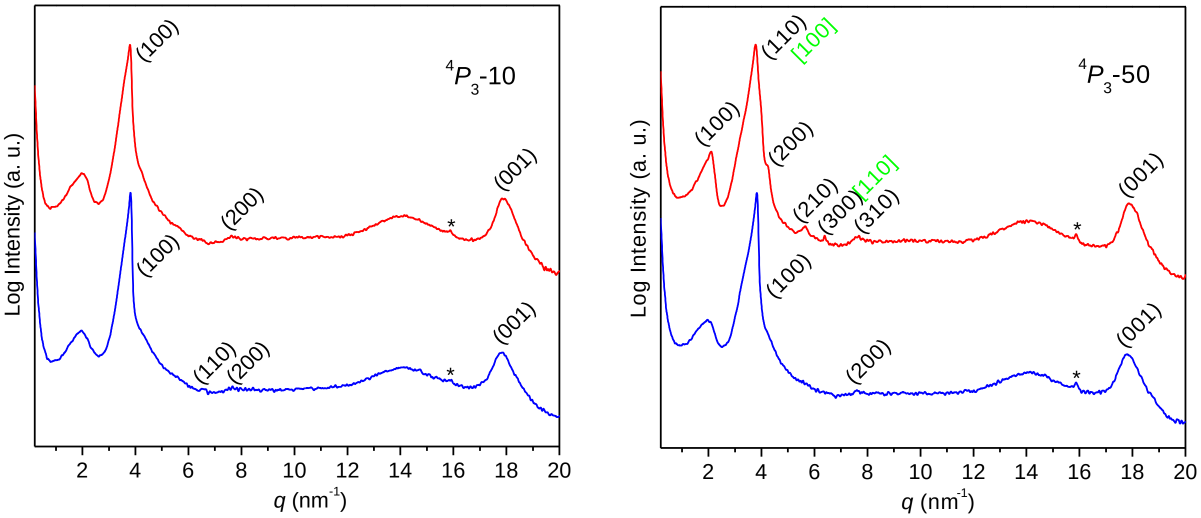

Figure S9. SAXS/WAXS patterns of $^4P_3$-10 and $^4P_3$-50 with proposed indexing at 50 °C on cooling from isotropic melts at a rate of 10 °C min^{-1} (blue lines) or after a stepwise cooling process (red lines).

Table S5. Representative SAXS/WAXS data for $^4P_3$-50 at 50 °C on cooling from isotropic melt at a rate of 10 °C min^{-1} (Col$_h$) or after a stepwise cooling process (Col$_{h\text{-}s}$).

Meso-phase	*hkl*	d_{obs} [Å]	d_{calc} [Å]	Lattice parameter [Å]	ρ_{calc}[a] [g cm^{-3}]
Col$_{h\text{-}s}$	100	29.4	29.4		
(50 °C)	110[100][b]	16.7	16.9	a = 33.9	1.02
$p3m1$	200	14.8	14.7		
	210	11.1	11.1		
	300[110][b]	9.83	9.80		
	310	8.16	8.15		
		4.4 (diffuse halo)			
	001	3.52			
Col$_h$	100	16.7	16.7		
(50 °C)	200	8.3	8.4	a = 19.3	1.05
$p6mm$		4.4 (diffuse halo)			
	001	3.53			

[a] Density, ρ, calculated as $\rho = M \cdot Z/(N_A \cdot V_{\text{unit cell}})$, $V_{\text{unit cell}} = a^2 c \sqrt{3}/2$, where c is experimentally measured d value of (001) scattering peak, M is the molecular weight of the repeat unit of 717 g mol^{-1}, and Z = 3 (Col$_{h\text{-}s}$) or 1 (Col$_h$). [b] The green indexing in brackets indicated the coexisting hexagonal columnar lattice superposed on the hexagonal columnar superlattice Col$_{h\text{-}s}$ based on three-column bundles (deduced from calculated Z = 3 of Col$_{h\text{-}s}$).

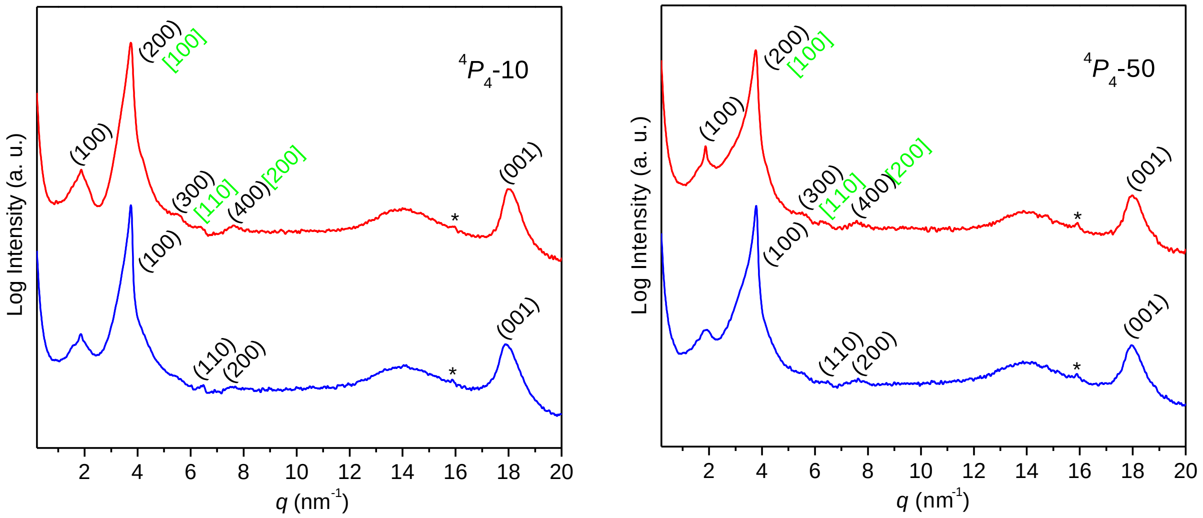

Figure S10. SAXS/WAXS patterns of $^4P_4$-10 and $^4P_4$-50 with proposed indexing at 50 ℃ on cooling from isotropic melts at a rate of 10 ℃ min^{-1} (blue lines) or after a stepwise cooling process (red lines).

Table S6. Representative SAXS/WAXS data for $^4P_4$-50 at 50 ℃ on cooling from isotropic melt at a rate of 10 ℃ min^{-1} (lower, Col$_h$) or after a stepwise cooling process (upper, Col$_h$/L).

Meso-phase	*hkl*	d_{obs} [Å]	d_{calc} [Å]	Lattice parameter [Å]	ρ_{calc}[a] [g cm^{-3}]
Col$_h$/L	100	33.4	33.4		
(50 °C)	200[100][b]	16.7	16.7	L = 33.4	1.08
*p*1	300	11.1	11.1	a'=19.3[b]	
	[110][b]	9.71	9.64		
	400[200][b]	8.33	8.35		
		4.5 (diffuse halo)			
	001	3.48			
Col$_h$	100	16.7	16.7		
(50 °C)	110	9.63	9.64	a = 19.3	1.08
*p*6*mm*	200	8.33	8.35		
		4.5 (diffuse halo)			
	001	3.49			

[a] Density, ρ, calculated as $\rho = M \cdot Z/(N_A \cdot V_{unit\ cell})$, $V_{unit\ cell} = a^2 c \cdot \sqrt{3}/2$, where c is experimentally measured d value of (001) scattering peak, M is the molecular weight of the repeat unit of 731 g mol^{-1}, and Z = 1. [b] The green indexing in brackets indicated the coexisting hexagonal columnar lattice superposed on the lamellar phase.

Both ${}^4P_3$-*n* and ${}^4P_4$-*n* series exhibited ordered Col$_h$ msophase with almost the same lattice parameter *a* = 19.3 Å on cooling from their isotropic melts at 10 ℃ min^{-1} (Figure S9, S10 and Table S5, S6). Moreover, a hexagonal columnar superlattice Col$_{h\text{-}s}$ with lattice parameter *a* = 33.9 Å was superposed on the hexagonal columnar lattice based on three-column bundles to form hierarchical structure (Figure 1 in the main text) as implied by the informative SAXS/WAXS patterns shown in Figure S9 for ${}^4P_3$-50 after a stepwise cooling process. The geometric considerations shown in Figure S8 also agree well with the structural elucidation from X-ray analysis. By contrast, the ${}^4P_4$-*n* series presented lamellar correlation besides hexagonal columnar lattice Col$_h$/L after a stepwise cooling process as shown in Figure S10 and Table S6. Such lamellar columnar phase may come from three-column bundles stacking mode as well but with alternately inverse orientations to organize into hexagonal columnar lattice based on side-chain TP stacking.[2] The absence of inter-lamellar correlation compared with that in ${}^4P_5$-50 allows slipping movement of three-column bundles within the horizontal direction and thus exhibits only lamellar electron density modulation with a period of √3 times larger than the primary hexagonal lattice parameter.

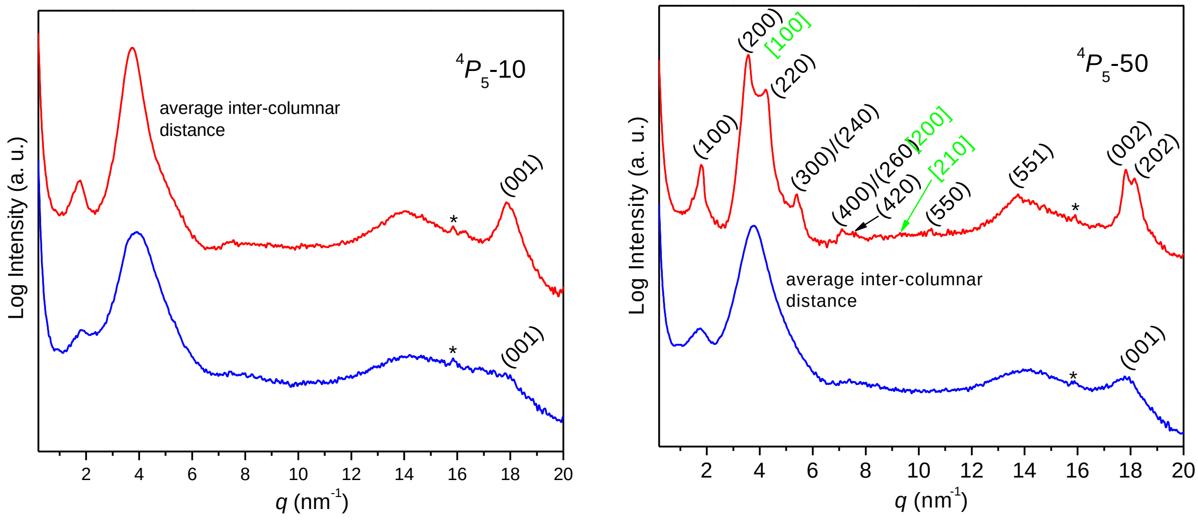

Figure S11. SAXS/WAXS patterns of ${}^4P_5$-10 and ${}^4P_5$-50 with proposed indexing at 50 ℃ on cooling from isotropic melts at a rate of 10 ℃ min^{-1} (blue lines) or after a stepwise cooling process (red lines).

Table S7. Representative SAXS/WAXS data for $^4P_5$-50 at 50 ℃ after a stepwise cooling process.

Meso-phase	hkl^b	d_{obs} [Å]	d_{calc} [Å]	Lattice parameter [Å]	$\rho_{calc}{}^a$ [g cm^{-3}]
	100	34.9	34.9		
Col$_{rp\text{-}s}$	200[100]^c	17.7	17.5	a = 34.9	1.00
(50 °C)	220	14.9	15.1	b = 60.4	
*p*2*mg*	300/240	11.6	11.6/11.4		
	400/260[200]^c	8.76	8.73/8.72		
	420	8.37	8.38		
	[210]^c	6.65	6.61		
	550	6.03	6.04		
	551	4.58	4.59		
		4.4 (diffuse halo)			
	002	3.53	3.53		
	202	3.46	3.46		

[a] Density, ρ, calculated as $\rho = M Z/(N_A \cdot V_{\text{unit cell}})$, $V_{\text{unit cell}} = a^2 c\cdot\sqrt{3}/2$, where c is experimentally measured d value of (002) scattering peak, M is the molecular weight of the repeat unit of 745 g mol^{-1}, and Z = 6. [b] The extinction rule of a 2D rectangular *p*2*mg* lattice is (0k): $k = 2i + 1$, and i is an integer. [c] The green indexing in brackets indicated the coexisting hexagonal columnar lattice superimposed on the rectangular columnar superlattice Col$_{rp\text{-}s}$ based on three-column bundles.

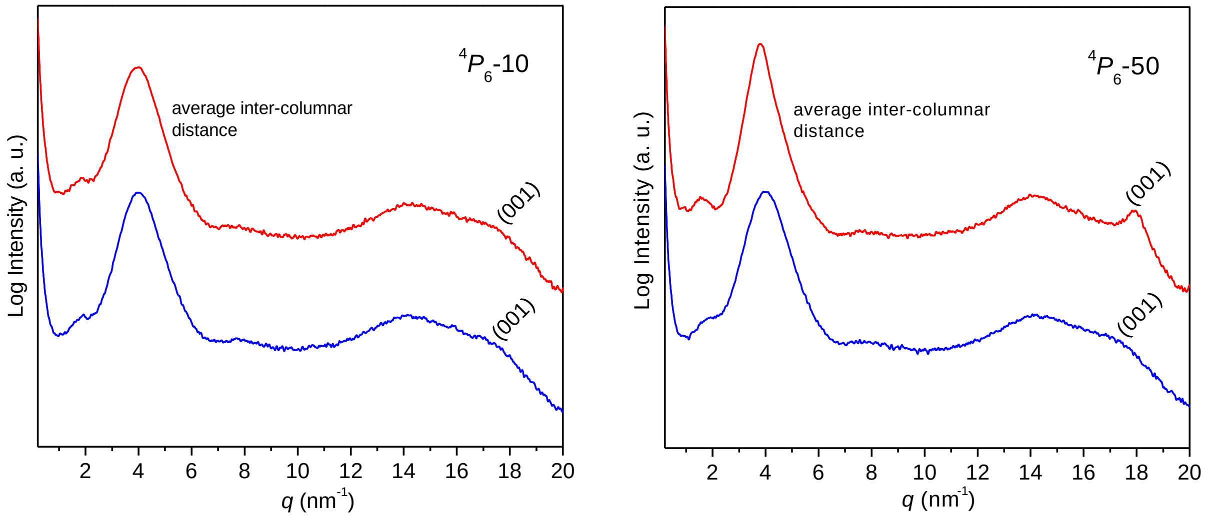

Figure S12. SAXS/WAXS patterns of $^4P_6$-10 and $^4P_6$-50 with proposed indexing at 50 ℃ on cooling from isotropic melts at a rate of 10 ℃ min^{-1} (blue lines) or after a stepwise cooling process (red lines).

Upon further elongation of spacer lengths, ${}^{4}P_{5}$-*n* and ${}^{4}P_{6}$-*n* only displayed unidentified columnar structures Col$_x$ with weak inter-columnar correlation upon cooling at 10 ℃ min^{-1} or after a stepwise cooling process from isotropic melts with an exception of ${}^{4}P_{5}$-50 (Figure S11, S12). The high-molecular-weight ${}^{4}P_{5}$-50 surprisingly exhibited rectangular columnar plastic superlattice Col$_{\text{rp-s}}$ with lattice parameter *a* = 34.9 Å and *b* = 60.4 Å superimposed on hexagonal columnar lattice based on three-column bundles undergoing a thermal annealing of stepwise cooling process (Figure S11, Table S7).

Table S8. Intra-columnar or Inter-columnar correlation lengths of ${}^{4}P_{m}$-50 at 50 ℃.

Polymer code	d_{intra}[a] [Å]	ξ_1[b] [Å]	N_1[c]	d_{inter}[a] [Å]	ξ_2[b] [Å]	N_2[c]
${}^{4}P_{1}$-50	3.53	180	51	18.4	898	49
${}^{4}P_{2}$-50	3.53	322	91	18.6	785	42
${}^{4}P_{3}$-50	3.52	190	54	19.3	496	26
${}^{4}P_{4}$-50	3.48	199	57	19.3	523	27
${}^{4}P_{5}$-50	3.46	393	113	20.1	314	15
${}^{4}P_{6}$-50	3.51	195	56	19.0	135	7

[a] Intra- or inter-columnar distance (*d*) determined by X-ray scattering analysis. [b] 1D intra-columnar (ξ_1) or 2D inter-columnar (ξ_2) correlation length evaluated through Scherrer equation. [c] The corresponding number of TP discotic units within a 1D column or number of columns in a 2D lattice.

It should be pointed out that the temperature 50 ℃ for the SAXS/WAXS analyses of most polymer samples after a stepwise cooling process is some different from the temperature 25 ℃ employed for TOF measurements. Such a commonly adopted little higher temperature of 50 ℃ significantly facilitates temperature control and experimental operation, based on the two separate heating stages with temperature control range, respectively, of -20~120 ℃ and 50~300 ℃ associated with our X-ray instrument. As shown in Figure S3a, all the series ^4P_m-n after a stepwise cooling process exhibited no detectable phase transitions below their isotropization temperatures. Moreover, variable temperature SAXS/WAXS analyses presented almost identical patterns, as shown in Figure S13 for the representative sample $^4P_2$-50, manifesting their unchanged structures at around room temperature and our commonly adopted temperature 50 ℃ for the SAXS/WAXS measurements. Therefore, structure-mobility correlations can be established despite small differences in measured temperatures.

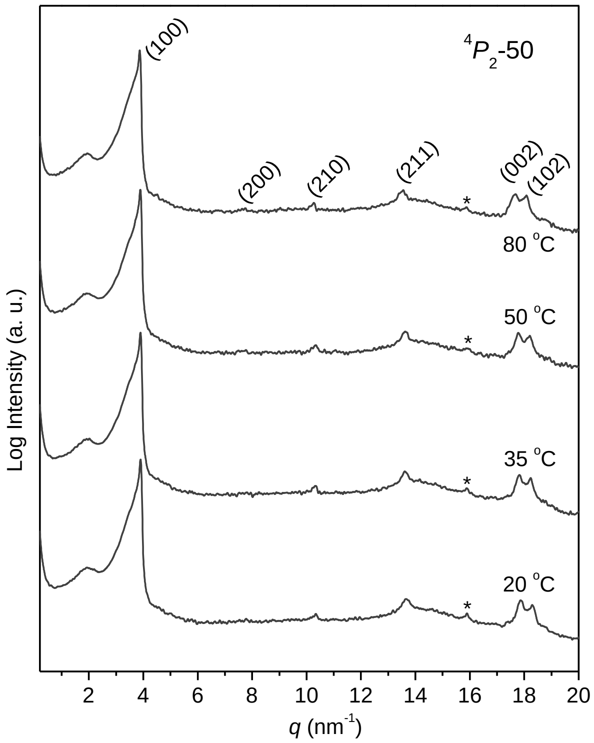

Figure S13. Variable temperature SAXS/WAXS patterns of $^4P_2$-50 with proposed indexing at indicated temperatures during a heating process after stepwise cooling from its isotropic melt, showing almost identical patterns manifesting the unchanged structure at around room temperature and the commonly adopted temperature 50 ℃ for the SAXS/WAXS measurements of most samples after a stepwise cooling process.

4. Variant discotic columnar stacking modes in columnar LC mesophases or columnar plastic phases

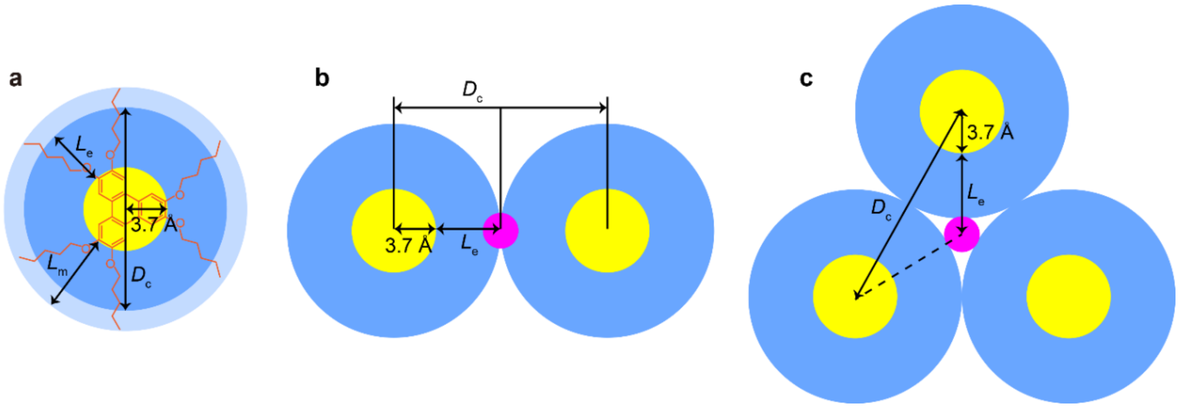

Figure S14. Schematic illustration of (a) columnar organization of hexa-alkyloxy substituted TP discotic molecules for calculating length shrinkage ratio (LSR) of peripheral alkyl tails, and (b,c) columnar arrangements in side-chain DLC polymers for estimating LSR of their flexible spacers based on (b) two-column bundles and (c) three-column bundles stacking mode, in top view.

$$\mathrm{LSR} = (L_m - L_e)/L_m \tag{S1}$$

$$L_e = D_c/2 - 3.7\ \text{Å} \tag{S2}$$

$$L_e = D_c/\sqrt{3} - 3.7\ \text{Å} \tag{S3}$$

Wherein, LSR indicates length shrinkage ratio of peripheral flexible alkyl tails of hexa-alkyloxy substituted TPs or spacers in DLC polymers. L_m is the maximum theoretical length in an *all-trans* conformation estimated from ChemBio3D Ultra 11.0; L_e is experimentally determined length according to Equation (S2) and (S3); D_c is the columnar diameter determined by X-ray scattering analysis.

Both the whole discotic unit and rigid aromatic TP core are regarded as approximately circular discs for building up simplified simulation model (Figure S14), where the average radius of TP core is 3.7 Å, thus the dimensions of the whole discotic units vary with the length of peripheral alkyl chains. The Equation (S2) is used for calculating L_e values of alkyl tails (Figure S14a) or spacers of polymers in two-column bundles organization mode (Figure S14b), while Equation (S3) for spacers of polymers in three-column bundles based cases (Figure S14c). The D_c values for hexa-alkyloxy substituted TPs are determined referred to Reference 3,4, and for polymer systems are deduced from X-ray scattering analysis results as discussed in the preceding section. The changing tendency and comparison of LSR dependence on alkyl chain length is shown in Figure S15.

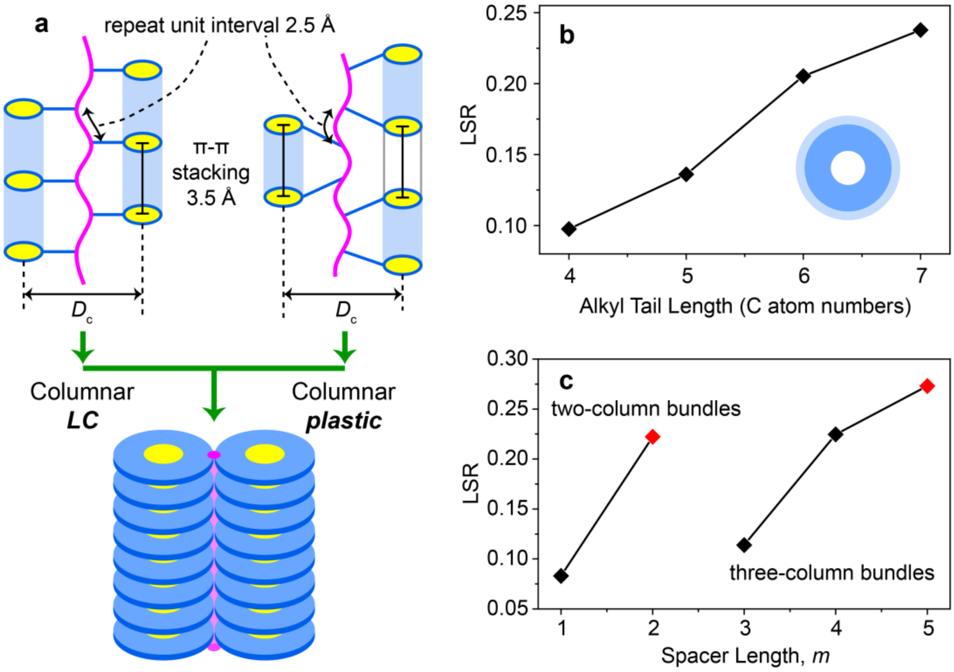

Figure S15. (a) Schematic illustration of different stacking modes of side-chain TP units within the columns of columnar LC mesophase by individual discs and of columnar plastic phase by disc pairs, with the cartoon picture at bottom only showing the same opposite direction stacking scenario while not reflecting their possible order difference. (b,c) Dependence of LSR on the chain length (carbon atom or methylene numbers) for (b) peripheral alkyl tails of hexa-alkyloxy substituted TPs and (c) polymethylene spacers linking side-chain discotic TP units and polymer backbone in DLC polymer systems.

Only high-MW polymers $^4P_2$-50 and $^4P_5$-50 display 3D positionally ordered columnar plastic phases, which seems reasonable from geometric dimensions consideration, also supported by comparative analysis of the alkyl chain shrinking performance. First, noteworthy is that the intra-columnar repeat distance for columnar plastic phase is twice of that found for the normal columnar LC phase, a unique feature shown by the samples in this article, as well as reported in other publications,[5-7] apparently indicating a corresponding intra-columnar correlation of disc pairs.[5-7] In our previous reports,[1,2] a discrete columnar stacks (DCS) based stacking mode has been proposed for

^6P_m-n series with intermediate spacer lengths, that a certain number of neighboring TP units of the same polymer chain self-assemble into a DCS subunit, then a supercylinder is constructed with the DCS subunits surrounding the polymer backbone, which further self-organizes into extended columns with 2D inter-columnar order to achieve variant columnar superstructures.[1] Here in this work, a similarly discrete stacking mode but with side-chain TP pairs as the stacking subunits accounts well for the formation of columnar plastic phases (Figure S15a). It is necessary for alkyl chains to shrink in LC assemblies especially for longer chains higher length shrinkage ratio (LSR) are required, as illustrated in Figure S15b of alkyl tails LSR versus the chain length represented by carbon atom numbers of hexa-alkyloxy substituted TPs. Such shrinking tendency of alkyl spacers for the whole polymers ^4P_m-n is remarkable, especially a monotonic increase for the subdivisional group samples with the same organization mode presents as shown in Figure S15c, with the red symbols indicating the formation of columnar plastic phase for high-MW polymers. Because of the main chain repeat unit interval 2.5 Å smaller than the average inter-disc distance 3.5 Å within a column, therefore, the formation of polymeric columnar plastic phase adopting discrete TP pairs stacking mode requires longer spacer or higher LSR for spacer than that in columnar LC phase with normally stacked individual TP discs, so as to allow spacer curving adaption along columns to some extent (Figure S15a). Therefore, $^4P_2$-50 with higher LSR than $^4P_1$-50 produce columnar plastic phase in the two-column bundles stacking group; while for three-column bundles stacking mode, only the polymer $^4P_5$-50 possessing the highest LSR even more than $^4P_2$-50 can organize into columnar plastic phase, in agreement with the general trend illustrated above of longer chains generating higher LSR. Furthermore, thanks to the side-chain TP discs piling up along the polymer main chain direction, such arrangement will in turn facilitate orientational correlation of discotic columns,[1,2,8,9] therefore, high-MW polymers with larger orientational association capability of side-chain discotic units than low-MW oligomers facilitate the formation of highly ordered columnar plastic phases.

5. Some supplementary POM images

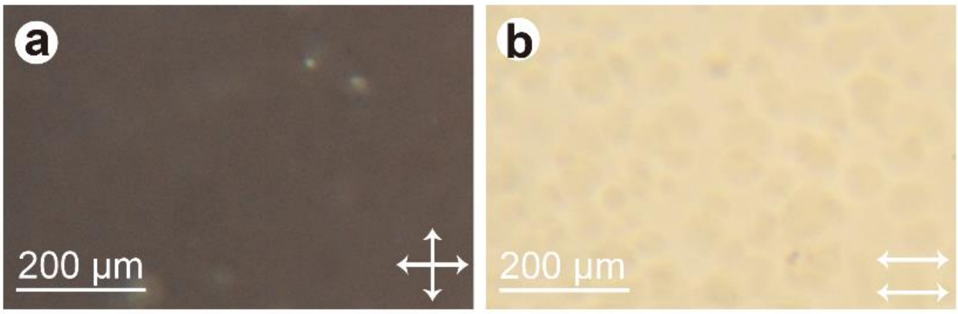

Figure S16. Optical microscopy images of $^{4}P_{2}$-50 sandwiched between two glass plates taken at 150 ℃ during very slowly cooling from its isotropic melt.

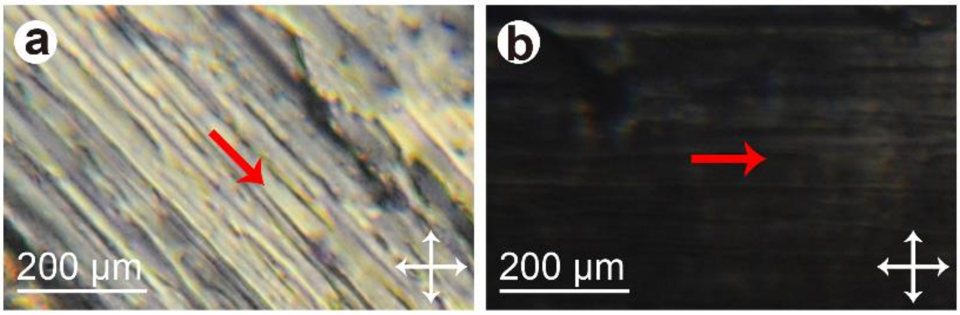

Figure S17. Optical microscopy images of $^{4}P_{2}$-50 sandwiched between two glass plates produced by shearing its concentrated hexane solution.

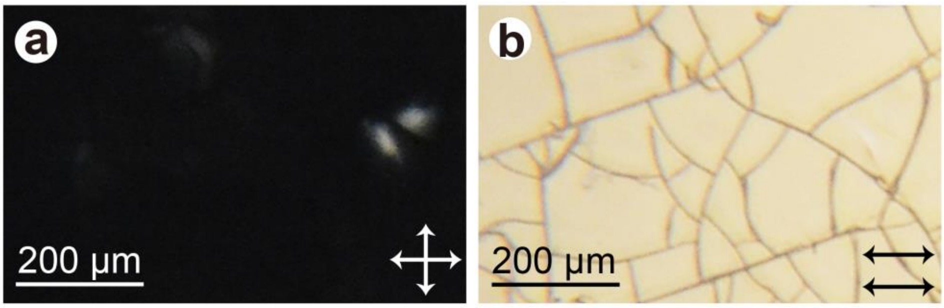

Figure S18. Directly photographed optical microscopy images of $^{4}P_{2}$-50 at 25 ℃ in a LC cell with coated semi-transparent indium tin oxide (ITO) employed for charge-carrier mobility measurements with the polarizer and analyzer (a) in orthogonal, or (b) in parallel with each other.

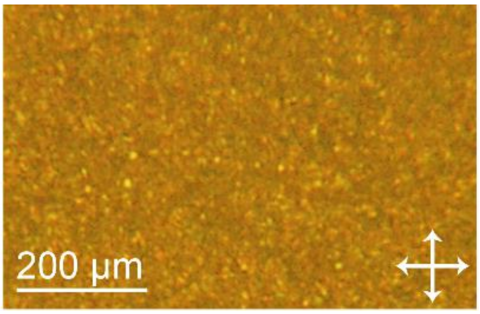

Figure S19. Optical microscopy images of ${}^{4}P_{5}$-50 sandwiched between two glass plates after a slowly cooling process from its isotropic melt.

6. Charge-carrier mobility measurements by TOF

Hole mobilities μ at zero electric field ($E = 0$) were estimated by extrapolation from the plots of the corresponding mobilities as a function of $E^{1/2}$, assuming the charge carrier transporting in a disordered manner, where mobility μ is defined by the following equation:[10,11]

$$\mu = \mu_0 \exp[-(2\sigma/3kT)^2]\exp\{CE^{1/2}[(\sigma/kT)^2 - \Sigma^2]\}$$

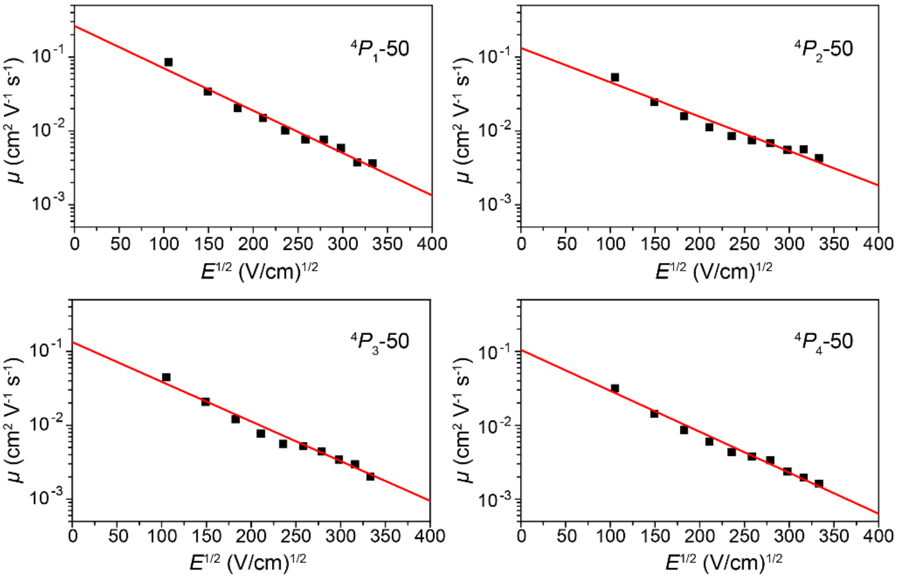

Figure S20. Electric field E dependence of the charge carrier mobilities of DLC polymers ${}^{4}P_{m}$-50 as a function of $E^{1/2}$ assuming a disordered transporting manner.

7. Supplementary references

1 B. Mu, B. Wu, S. Pan, J. L. Fang and D. Z. Chen, *Macromolecules*, 2015, **48**, 2388-2398.

2 B. Mu, S. Pan, H. F. Bian, B. Wu, J. L. Fang and D. Z. Chen, *Macromolecules*, 2015, **48**, 6768-6780.

3 S. K. Prassad, D. S. S. Rao, S. Chandrasekhar and S. Kumar, *Mol. Cryst. Liq. Cryst.*, 2003, **396**, 121-139.

4 J. Simmerer, B. Glusen, W. Paulus, A. Kettner, P. Schuhmacher, D. Adam, K. H. Etzbach, K. Siemersmeyer, J. H. Wendorff, H. Ringsdorf and D. Haarer, *Adv. Mater.*, 1996, **8**, 815-819.

5 B. Gluesen, W. Heitz, A. Kettner and J. H. Wendorff, *Liq. Cryst.*, 1996, **20**, 627-633.

6 W. Fimmen, B. Glusen, A. Kettner, M. Wittenberg and J. H. Wendorff, *Liq. Cryst.*, 1997, **23**, 569-573.

7 B. Glusen, A. Kettner and J. H. Wendorff, *Mol. Cryst. Liq. Cryst. Sci. Technol., Sect. A: Mol. Cryst. Liq. Cryst.*, 1997, **303**, 115-120.

8 B. Hueser, T. Pakula and H. W. Spiess, *Macromolecules*, 1989, **22**, 1960-1963.

9 D. Stewart, G. S. McHattie and C. T. Imrie, *J. Mater. Chem.*, 1998, **8**, 47-51.

10 H. Bässler, *Phys. Status Solidi B*, 1993, **175**, 15-56.

11 M. Van der Auweraer, F. C. De Schryver, P. M. Borsenberger and H. Bässler, *Adv. Mater.*, 1994, **6**, 199-213.